 CMES, vol.48, no.1, pp.1-26, 2009

Fracture Analysis for Two-dimensional Plane Problems of Nonhomogeneous Magneto-electro-thermo-elastic Plates Subjected to Thermal Shock by Using the Meshless Local Petrov-Galerkin Method

W. J. Feng[1], X. Han[2] and Y.S. Li[3]

Abstract: The two-dimensional (2D) fracture problem of nonhomogeneous magneto-electro-thermo-elastic materials under dynamically thermal loading is investigated by the meshless local Petrov-Galerkin (MLPG) method. The material parameters are assumed to vary in either the height or width direction of the plates. The Laplace-transform technique is utilized to solve the time-dependent problems. In this MLPG analysis, the moving least squares (MLS) method is adopted to approximate the physical quantities, and the Heaviside step function is taken as a test function. The validity and efficiency of the MLPG method are firstly examined. The crack problem of a nonhomogeneous magneto-electro-thermo-elastic plate is then considered. The field intensity factors (FIFs) including the stress intensity factor (SIF), electric displacement intensity factor (EDIF), magnetic induction intensity factor (MIIF) and mechanical mode-I strain energy release rate (MSERR) of the magneto-electro-thermo-elastic materials are computed. The effects of the nonhomogeneous parameters especially the thermal nonhomogeneous parameters on the fracture behavior of crack tips are emphatically evaluated and discussed according the energy release rate criterion. The results seem useful for the design of nonhomogeneous material worked in high or low temperature environments.

Keywords: meshless local Petrov-Galerkin method, magneto-electro-thermo-elastic materials, nonhomogeneous plates, field intensity factors, fracture mechanics

[1] Department of Engineering Mechanics, Shijiazhuang Railway Institute, Shijiazhuang 050043, P.R. China. Correspondence author. *E-mail address:* wjfeng999@yahoo.com (W.J. Feng)

[2] State Key Lab Adv Design & Manufacture Vehicle Bo, Hunan University, Changsha 410082, P.R. China

[3] Institute of Engineering Mechanics, Northeastern University, Shenyang 110004, P.R. China

1 Introduction

Magnetoelectroelastic materials have been found wide engineering applications for their mechanical-electrical-magnetic coupling effect. This begins with the work of Van Suchtelen (1972), who proposed that the combination of piezoelectric-piezomagnetic phase may exhibit a new material property - the magnetoelectric coupling effect. Since then, much of the theoretical studies have been carried out [Avellaneda and Harshe (1994); Benveniste (1995); Li (2000); Nan (1994); Huang and Kuo (1997)].

On the other hand, magnetoelectroelastic materials have a tendency to develop critical cracks during the manufacturing and poling process. And the fracture behaviors of the materials for both the static crack problems [Gao et al. (2003a,b); Song and Sih (2003); Tian and Gabbert (2004); Zhou et al. (2005); Zhao et al. (2006); Wang and Mai (2007)] and dynamic crack problems [Li (2005); Feng et al. (2007); Feng and Pan (2008)] have been investigated. In addition, heating or nonuniform temperature fields can also reduce the service life of these kinds of materials and structures or make them failure especially as they operate at high or low temperature environments. However, up till now, the thermal effects related to cracks in magnetoelectroelastic materials are reported only in several literatures [Gao et al. (2003c); Niraula and Wang (2006); Feng et al. (2008)]. Among these papers, Gao et al. (2003c) analyzed the collinear permeable-crack problems of infinite magneto–electro–thermo-elastic materials. Niraula and Wang (2006) obtained the exact solution of penny-shaped crack problem in an infinite magnetoelectroelastic medium under uniform heat flow. Feng et al. (2008) studied the mechanical behavior induced by a penny-shaped crack in a finite magneto-electro-thermal-elastic layer subjected to a heat flow. It should be pointed out that the work on fracture analysis for nonhomogenous magnetoelectroelastic materials under thermal loading has not been addressed and that it is much complicated to get the corresponding analysis solution because of the mathematical difficulty. Thus, numerical method is an important tool to investigate this kind of problems.

Recently, considerable research in computational mechanics has been devoted to the development of meshless methods since it does not require a mesh to discretize the problem domain, and the approximate solution is constructed entirely in terms of a set of scattered nodes. The meshless local Petrov-Galerkin (MLPG) method is proposed by Atluri and Zhu (1998), which is based on local weak forms of governing equations and employs meshless interpolations for both the trial and test functions. The trial functions are generally constructed by using the moving least squares (MLS) approximation. These approximations simply rely on the location of points or nodes in the body, rather than complex meshes [Lancaster and Salkauskas (1981)]. In the Petrov-Galerkin formulation, the test functions may be cho-

sen from a space different from the space of trial functions [Atluri et al. (1999)]. It should be noted that depending on the weak formulation's test functions of the MLPG method, Atluri and coworkers developed six different MLPG methodologies [Atluri and Shen (2002a); Atluri and Shen (2002b)]

The MLPG method has been successfully applied to several kinds of problems including elasto-statics [Li et al. (2003); Han and Atluri (2003); Han and Atluri (2004a); Sellountos et al. (2005)], elasto-dynamics [Han and Atluri (2004b)], impact problems [Han et al. (2006)], shell problems [Sladek et al. (2006a); Jarak et al. (2007)], heat conduction problems [Sladek et al. (2008a)], fracture problems [Batra and Ching (2002); Gao et al. (2006); Sladek et al. (2007a); Long et al. (2008)], thermoelastic problems [Qian and Batra (2005); Ching and Yen (2005); Ching and Chen (2006); Sladek et al.(2006b)], thermo-piezoelectric and axisymmetric piezoelectric problems [Sladek et al. (2007b); Sladek et al. (2008b)], and magneto-electro-elastic problems [Sladek et al. (2008c)]. A comprehensive presentation on the application of the MLPG method to different types of boundary value problems can be found in the book of [Atluri (2004)]. However, to date, to the best of our knowledge, no report is presented on the nonhomogeneous magneto-electro-thermo-elastic fracture problem, let alone by the MLPG method.

This paper aims to investigate the two-dimensional (2D) fracture problems of nonhomogeneous magneto-electro-thermo-elastic materials under thermal loading by the MLPG method. In this MLPG analysis, the MLS method is adopted to approximate the physical quantities, and the Heaviside step function is taken as a test function. The validity and efficiency of the MLPG method are firstly examined, and the stress intensity factor (SIF), electric displacement intensity factor (EDIF), magnetic induction intensity factor (MIIF) and mechanical mode-I strain energy release rate (MSERR) of the magneto-electro-thermo-elastic plates are computed and further analyzed.

2 Fundamental equations of magneto-electro-thermo-elasticity

For a nonhomogeneous magneto-electro-thermo-elastic solid, the constitutive equations related the mechanical stresses σ_{ij}, electric displacements D_i and magnetic inductions B_i with the elastic strains γ_{ij}, electric fields E_i, magnetic fields H_i and temperature increment θ are given by Huang and Kuo (1997)

$$\sigma_{ij}(x,t) = c_{ijkl}(x)\gamma_{kl}(x,t) - e_{kij}(x)E_k(x,t) - f_{kij}(x)H_k(x,t) - \lambda_{ij}(x)\,\theta(x,t) \tag{1a}$$

$$D_i(x,t) = e_{ikl}(x)\gamma_{kl}(x,t) + \varepsilon_{ik}(x)E_k(x,t) + g_{ik}(x)H_k(x,t) + p_i(x)\theta(x,t) \tag{1b}$$

$$B_i(x,t) = f_{ikl}(x)\gamma_{kl}(x,t) + g_{ik}(x)E_k(x,t) + \mu_{ik}(x)H_k(x,t) + m_i(x)\theta(x,t) \tag{1c}$$

where c_{ijkl}, ε_{ik} and μ_{ik} denote the elastic stiffnesses, dielectric permittivities and magnetic permeabilities, respectively; e_{kij}, f_{kij} and g_{ik} are the piezoelectric, piezomagnetic and magnetoelectric coupling coefficients, respectively; λ_{ij}, p_i and m_i are the thermal modules, pyroelectric and pyromagnetic constants, respectively. x and t denote the coordinate and time, respectively.

The Fourier's heat conduction law can be expressed as

$$q_i(x,t) = -k_{ij}(x)\theta_{,j}(x,t) \tag{2}$$

where q_i and k_{ij} are the heat fluxes and thermal conductivities, respectively. Subscript comma denotes the partial differentiation with respect to the coordinate.

The elastic strains γ_{ij}, electric fields E_i, magnetic fields H_i are related to the displacements u_i, electric potential ϕ and magnetic potential ψ by

$$\gamma_{kl}(x,t) = [u_{i,j}(x,t) + u_{j,i}(x,t)]/2 \tag{3a}$$

$$E_i(x,t) = -\phi_{,i}(x,t) \tag{3b}$$

$$H_i(x,t) = -\psi_{,i}(x,t) \tag{3c}$$

In the absence of body forces, free charges and internal heat generation, the mechanical, electromagnetic and heat equilibrium equations of magneto-electro-thermo-elasticity are

$$\sigma_{ij,j}(x,t) = \rho(x)\ddot{u}_i(x,t) \tag{4a}$$

$$D_{j,j}(x,t) = 0 \tag{4b}$$

$$B_{j,j}(x,t) = 0 \tag{4c}$$

$$[k_{ij}(x,t)\,\theta_{,i}(x,t)]_{,j} = \rho(x)c(x)\dot{\theta}(x,t) \tag{4d}$$

where ρ and c are, respectively, the mass density and specific heat. The dots over a quantity indicate the time derivative.

For 2D plane strain problem, the constitutive equations can be written as

$$\begin{Bmatrix}\sigma_{11}\\ \sigma_{33}\\ \sigma_{13}\end{Bmatrix} = \begin{bmatrix}c_{11} & c_{13} & 0\\ c_{13} & c_{33} & 0\\ 0 & 0 & c_{44}\end{bmatrix}\begin{Bmatrix}\gamma_{11}\\ \gamma_{33}\\ 2\gamma_{13}\end{Bmatrix} - \begin{bmatrix}0 & e_{31}\\ 0 & e_{33}\\ e_{15} & 0\end{bmatrix}\begin{Bmatrix}E_1\\ E_3\end{Bmatrix} - \begin{bmatrix}0 & f_{31}\\ 0 & f_{33}\\ f_{15} & 0\end{bmatrix}\begin{Bmatrix}H_1\\ H_3\end{Bmatrix} - \begin{Bmatrix}\lambda_{11}\\ \lambda_{33}\\ 0\end{Bmatrix}\theta$$
$$= \mathbf{c}\gamma - \mathbf{e}E - \mathbf{f}H - \lambda\theta \tag{5a}$$

$$\begin{Bmatrix} D_1 \\ D_3 \end{Bmatrix} = \begin{bmatrix} 0 & 0 & e_{15} \\ e_{31} & e_{33} & 0 \end{bmatrix} \begin{Bmatrix} \gamma_{11} \\ \gamma_{33} \\ 2\gamma_{13} \end{Bmatrix} + \begin{bmatrix} \varepsilon_{11} & 0 \\ 0 & \varepsilon_{33} \end{bmatrix} \begin{Bmatrix} E_1 \\ E_3 \end{Bmatrix} + \begin{bmatrix} g_{11} & 0 \\ 0 & g_{33} \end{bmatrix} \begin{Bmatrix} H_1 \\ H_3 \end{Bmatrix} + \begin{Bmatrix} p_1 \\ p_3 \end{Bmatrix} \theta = \mathbf{e}^T \gamma - \varepsilon E - \mathbf{g} H - p\theta \quad (5b)$$

$$\begin{Bmatrix} B_1 \\ B_3 \end{Bmatrix} = \begin{bmatrix} 0 & 0 & f_{15} \\ f_{31} & f_{33} & 0 \end{bmatrix} \begin{Bmatrix} \gamma_{11} \\ \gamma_{33} \\ 2\gamma_{13} \end{Bmatrix} + \begin{bmatrix} g_{11} & 0 \\ 0 & g_{33} \end{bmatrix} \begin{Bmatrix} E_1 \\ E_3 \end{Bmatrix} + \begin{bmatrix} \mu_{11} & 0 \\ 0 & \mu_{33} \end{bmatrix} \begin{Bmatrix} H_1 \\ H_3 \end{Bmatrix} + \begin{Bmatrix} m_1 \\ m_3 \end{Bmatrix} \theta = \mathbf{f}^T \gamma - \mathbf{g} E - \mu H - m\theta \quad (5c)$$

where the quantities described by standardized boldfaces stand for matrices and the ones by italic boldfaces stand for vectors.

The following essential and natural boundary conditions are assumed

$$u_i(x,t) = \tilde{u}_i(x,t), \quad x \in \Gamma_u \quad (6a)$$

$$t_i(x,t) = \sigma_{ij}(x,t) n_j(x) = \tilde{t}_i(x,t), \quad x \in \Gamma_t \quad (6b)$$

$$\phi(x) = \tilde{\phi}(x), \quad x \in \Gamma_\phi \quad (7a)$$

$$D_j(x) n_j(x) = \tilde{D}(x), \quad x \in \Gamma_Q \quad (7b)$$

$$\psi(x) = \tilde{\psi}(x), \quad x \in \Gamma_\psi \quad (8a)$$

$$B_j(x) n_j(x) = \tilde{B}(x), \quad x \in \Gamma_R \quad (8b)$$

$$\theta(x,t) = \tilde{\theta}(x,t), \quad x \in \Gamma_\theta \quad (9a)$$

$$q(x,t) = k_{ij}(x) \theta_{,i}(x,t) n_j(x) = \tilde{q}(x,t), \quad x \in \Gamma_q \quad (9b)$$

for the mechanical field, electrical field, magnetic field and thermal field, respectively. In Eqs. (6)-(9), Γ_u, Γ_ϕ, $\Gamma_\psi$and Γ_θ are the parts of the global boundary with the prescribed elastic displacements, electric potential, magnetic potential and temperature increment, respectively; and on Γ_t, Γ_Q, Γ_R and Γ_q, the stress, electric displacement, magnetic induction and heat flux are prescribed, respectively; n_j are the components of a unit vector outward normal at a point on the natural boundary. For the 2D plane strain problem, $i, j = 1, 3$.

The initial conditions for the mechanical and thermal fields are assumed as

$$u_i(x,0) = 0, \quad x \in \Omega \tag{10a}$$

$$\dot{u}_i(x,0) = 0, \quad x \in \Omega \tag{10b}$$

$$\theta(x,0) = 0, \quad x \in \Omega \tag{10c}$$

where Ω denotes the whole global domain.

3 Interpolation approximation

The MLS method is generally considered to be one of the best schemes to interpolate data with reasonable accuracy. Consider a domain Ω_x in the neighborhood of the point x. Ω_x is located within the problem domain Ω. The MLS approximate $U^h(x)$ of $U(x)$ in the subdomain Ω_x are defined by

$$U^h(x) = p^T(x)\mathbf{a}(x) \tag{11}$$

where $U^h(x)$ is the approximate function of extended displacement, and

$$U^h(x) = \left\{u_1^h(x) \quad u_3^h(x) \quad \phi^h(x) \quad \psi^h(x) \quad \theta^h(x)\right\} \tag{12a}$$

and $p(x)$ is a complete monomial basis function of order m, which can be expressed as

$$p^T(x) = \left\{1 \quad x_1 \quad x_3\right\}, \text{ for } m = 3 \tag{12b}$$

$$p^T(x) = \left\{1 \quad x_1 \quad x_3 \quad x_1^2 \quad x_1x_3 \quad x_3^2\right\}, \text{ for } m = 6 \tag{12c}$$

The coefficient matrix $\mathbf{a}(x)$ in Eq. (11) can be obtained by minimizing the following weighted L_2 norm:

$$J^k(x) = \sum_{i=1}^{n} w_i(x)\left[p^T(x_i)\,\mathbf{a}^k(x) - \hat{U}_i^k\right]^2 = \left[\mathbf{P}\cdot\mathbf{a}^k(x) - \hat{\mathbf{U}}^k\right]^T \mathbf{W}\left[\mathbf{P}\cdot\mathbf{a}^k(x) - \hat{\mathbf{U}}^k\right] \tag{13}$$

where $k = 1,2,\cdots,5$ denote the mechanical, electrical and magnetic components, respectively. $\mathbf{a}^k$ is the kth column of $\mathbf{a}$. $\hat{\mathbf{U}}^k$ is the kth column of $\hat{\mathbf{U}}$, which is the $n\times 5$ matrix with the element $\hat{U}_i$ corresponding to the fictitious extended displacement vector at node x_i. $\mathbf{P}$ is the $n\times m$ matrix composed by n vectors $p^T(x_i)$. $\mathbf{W}$ is a diagonal weighted $n\times n$ matrix, and the element $w_i(x)$ of which is the weight function associated with the node i. x_i denotes the value of x at node i. n is the number of

nodes in Ω_x. In this study, the following spline weight function is introduced [Krysl and Belytschko (1995)]

$$w_i(x) = \begin{cases} 1-6r^2+8r^3-3r^4 & 0 \le r \le 1 \\ 0 & r \ge 1 \end{cases} \tag{14}$$

where $r = \|x-x_i\|/d_{\max}$, $d_{\max}$ is the radius of the influence domain of point x. The choice of the shape of the influence domain can be arbitrary. In most cases, for simplicity, square domains or circular domains are adopted.

The minimization of $J^k(x)$ $(k = 1,2,\cdots,5)$ leads to the following relation

$$\mathbf{A}(x)\mathbf{a}(x) = \mathbf{B}(x)\hat{\mathbf{U}} \tag{15}$$

where $\mathbf{A}(\mathbf{x})$ and $\mathbf{B}(\mathbf{x})$ can, respectively, be expressed as

$$\mathbf{A}(x) = \mathbf{P}^T\mathbf{W}\mathbf{P} = \sum_{i=1}^{n} w_i(x)p(x_i)p^T(x_i) \tag{16a}$$

$$\mathbf{B}(x) = \mathbf{P}^T\mathbf{W} = [w_1(x)p(x_1), w_2(x)p(x_2), \cdots w_n(x)p(x_n)] \tag{16b}$$

Solving $\mathbf{a}(x)$ from Eq. (15) and substituting it into Eq. (11), the approximated function of the extended displacement can be obtained as

$$U^h(x) = \varphi(x)\hat{\mathbf{U}} \tag{17}$$

where

$$\varphi(x) = p^T(x)\mathbf{A}^{-1}(x)\mathbf{B}(x) \tag{18}$$

Thus, the mechanical displacement, electrical potential, magnetic potential and temperature increment in Ω can finally be written as

$$u^h(x) = \mathbf{\Phi}_1(x)\hat{u} \tag{19a}$$

$$\phi^h(x) = \Phi_2(x)\hat{\phi} \tag{19b}$$

$$\psi^h(x) = \Phi_2(x)\hat{\psi} \tag{19c}$$

$$\theta^h(x) = \Phi_2(x)\hat{\theta} \tag{19d}$$

where

$$u^h(x) = \left\{u_1^h(x) \quad u_3^h(x)\right\}^T \tag{20a}$$

$$\mathbf{\Phi}_1(x) = \begin{bmatrix} \Phi(x) & \mathbf{0} \\ \mathbf{0} & \Phi(x) \end{bmatrix} \tag{20b}$$

$$\Phi_2(x) = \Phi(x) \tag{20c}$$

$\Phi(x)$ is a corresponding row vector with N elements, and N is the total node number in Ω. If node i is in the influence domain of x, the corresponding element $\Phi^i(x) = \varphi^i(x)$; otherwise, $\Phi^i(x) = 0$. $\hat{u}$ is the corresponding column vector with $2N$ elements, and $\hat{\phi}$, $\hat{\psi}$ and $\hat{\theta}$ are the corresponding column vectors with N elements.

4 The MLPG formulation

Introduce the Laplace transform

$$L[f(x,t)] = \bar{f}(x,p) = \int_0^\infty f(x,t)\, e^{-pt} dt \tag{21}$$

where p is the Laplace transform parameter. Applying the Laplace transform to Eqs. (4), one obtains

$$\bar{\sigma}_{ij,j}(x,p) - \rho(x) p^2 \bar{u}_i(x,p) = 0 \tag{22a}$$

$$\bar{D}_{j,j}(x,p) = 0 \tag{22b}$$

$$\bar{B}_{j,j}(x,p) = 0 \tag{22c}$$

$$\left[k_{ij}(x)\bar{\theta}_{,i}(x,p)\right]_{,j} - \rho(x)c(x)p\bar{\theta}(x,p) = 0 \tag{22d}$$

Using the weighted residual method, the local weak-form of the governing equations in a subdomain Ω_s (which includes the node s) can be obtained as

$$\int_{\Omega_s} \left[\bar{\sigma}_{ij,j}(x,p) - \rho(x) p^2 \bar{u}_i(x,p)\right] u^*_{ik}(x) d\Omega = 0 \tag{23a}$$

$$\int_{\Omega_s} \bar{D}_{j,j}(x,p)\, v^*(x)\, d\Omega = 0 \tag{23b}$$

$$\int_{\Omega_s} \bar{B}_{j,j}(x,p)\, m^*(x)\, d\Omega = 0 \tag{23c}$$

$$\int_{\Omega_s} \left\{ \left[k_{ij}(x)\bar{\theta}_{,i}(x,p)\right]_{,j} - \rho(x)c(x)p\bar{\theta}(x,p) \right\} n^*(x)\, d\Omega = 0 \tag{23d}$$

where $u^*_{ik}(x)$,$v^*(x)$, $m^*(x)$ and $n^*(x)$ are the test functions of the mechanical, electric, magnetic and temperature fields in the Laplace domain, respectively. Applying the Gauss divergence theorem, Eqs. (23) can further be written as

$$\int_{\partial\Omega_s} \bar{\sigma}_{ij}(x,p)\, u^*_{ik}(x) n_j(x) d\Gamma - \int_{\Omega_s} \left[\bar{\sigma}_{ij}(x,p)\, u^*_{ik,j}(x) + \rho(x) p^2 \bar{u}_i(x,p)\, u^*_{ik}(x)\right] d\Omega = 0$$

(24a)

$$\int_{\partial\Omega_s} \bar{D}_j(x,p)\, v^*(x)\, n_j(x) d\Gamma - \int_{\Omega_s} \bar{D}_j(x,p)\, v^*_{,j}(x) d\Omega = 0 \tag{24b}$$

$$\int_{\partial\Omega_s} \bar{B}_j(x,p)\, m^*(x)\, n_j(x) d\Gamma - \int_{\Omega_s} \bar{B}_j(x,p)\, m^*_{,j}(x) d\Omega = 0 \tag{24c}$$

$$\begin{aligned}&\int_{\partial\Omega_s} k_{ij}(x)\bar{\theta}_{,i}(x,p)\, n^*(x) n_j(x) d\Gamma - \int_{\Omega_s} k_{ij}(x)\bar{\theta}_{,i}(x,p)\, n^*_{,j}(x) d\Omega \\ &- \int_{\Omega_s} \rho(x) c(x)\, p\bar{\theta}(x,p)\, n^*(x) d\Omega = 0\end{aligned} \tag{24d}$$

By choosing the Heaviside step function as the test functions in each subdomain, a system of linear algebraic equations yield from Eqs. (24)

$$\begin{bmatrix} \mathbf{K}^s_{mm}(x,p) & \mathbf{K}^s_{me}(x) & \mathbf{K}^s_{mg}(x) & -\mathbf{K}^s_{m\theta}(x) \\ K^s_{em}(x) & -K^s_{ee}(x) & -K^s_{eg}(x) & K^s_{e\theta}(x) \\ K^s_{gm}(x) & -K^s_{ge}(x) & -K^s_{gg}(x) & K^s_{g\theta}(x) \\ \mathbf{0} & \mathbf{0} & \mathbf{0} & -K^s_{\theta\theta}(x,p) \end{bmatrix} \begin{Bmatrix} \hat{u}^s(p) \\ \hat{\phi}^s(p) \\ \hat{\psi}^s(p) \\ \hat{\theta}^s(p) \end{Bmatrix} = \begin{Bmatrix} F^s_m(x,p) \\ F^s_e(x,p) \\ F^s_g(x,p) \\ F^s_\theta(x,p) \end{Bmatrix} \tag{25}$$

where

$$\mathbf{K}^s_{mm}(x,p) = \int_{L_s+\Gamma_{su}} \mathbf{N}_1(x)\mathbf{c}(x)\mathbf{B}_1(x)\, d\Gamma - \int_{\Omega_s} \rho(x)\, p^2 \mathbf{I}\boldsymbol{\Phi}_1(x) d\Omega \tag{26a}$$

$$\mathbf{K}^s_{me}(x) = \int_{L_s+\Gamma_{su}} \mathbf{N}_1(x)\mathbf{e}(x)\mathbf{B}_2(x)\, d\Gamma \tag{26b}$$

$$\mathbf{K}^s_{mg}(x) = \int_{L_s+\Gamma_{su}} \mathbf{N}_1(x)\mathbf{f}(x)\mathbf{B}_2(x)\, d\Gamma \tag{26c}$$

$$\mathbf{K}^s_{m\theta}(x) = \int_{L_s+\Gamma_{su}} \mathbf{N}_1(x)\boldsymbol{\lambda}(x)\Phi_2(x)\, d\Gamma \tag{26d}$$

$$K^s_{em}(x) = \int_{L_s+\Gamma_{s\phi}} N_2(x)\, \mathbf{e}^T(x)\mathbf{B}_1(x)\, d\Gamma \tag{26e}$$

$$K^s_{ee}(x) = \int_{L_s+\Gamma_{s\phi}} N_2(x)\, \boldsymbol{\varepsilon}(x)\mathbf{B}_2(x)\, d\Gamma \tag{26f}$$

$$K^s_{eg}(x) = \int_{L_s+\Gamma_{s\phi}} N_2(x)\, \mathbf{g}(x)\mathbf{B}_2(x) d\Gamma \tag{26g}$$

$$K^s_{e\theta}(x) = \int_{L_s+\Gamma_{s\phi}} N_2(x)\, p(x)\Phi_2(x) d\Gamma \tag{26h}$$

$$K^s_{gm}(x) = \int_{L_s+\Gamma_{s\psi}} N_2(x)\,\mathbf{f}^T(x)\mathbf{B}_1(x)\,d\Gamma \tag{26i}$$

$$K^s_{ge}(x) = \int_{L_s+\Gamma_{s\psi}} N_2(x)\,\mathbf{g}(x)\mathbf{B}_2(x)d\Gamma \tag{26j}$$

$$K^s_{gg}(x) = \int_{L_s+\Gamma_{s\psi}} N_2(x)\,\mu(x)\mathbf{B}_2(x)d\Gamma \tag{26k}$$

$$K^s_{g\theta}(x) = \int_{L_s+\Gamma_{s\psi}} N_2(x)\,m(x)\Phi_2(x)d\Gamma \tag{26l}$$

$$K^s_{\theta\theta}(x,p) = \int_{L_s+\Gamma_{s\theta}} N_2(x)\mathbf{k}(x)\mathbf{B}_2(x)\,d\Gamma - \int_{\Omega_s} \rho(x)c(x)\,p\Phi_2(x)d\Omega \tag{26m}$$

with Γ being the local boundary totally inside the global domain. $\Gamma_{s\mathbf{u}}$, $\Gamma_{s\phi}$, $\Gamma_{s\psi}$ and $\Gamma_{s\theta}$ are the parts of the local boundaries which coincide with the global elastic displacement, electric potential, magnetic potential and temperature increment boundaries, respectively. $\mathbf{k}(x)$ is the matrix of thermal conductivity. $\mathbf{I}$ is the unit matrix defined by

$$\mathbf{I} = \begin{bmatrix} 1 & 0 \\ 0 & 1 \end{bmatrix} \tag{27}$$

$\mathbf{N}_1(x)$ and $N_2(x)$ are related to the normal vector $n_j(x)$ on $\partial\Omega_s$ by

$$\mathbf{N}_1(x) = \begin{bmatrix} n_1(x) & 0 & n_2(x) \\ 0 & n_2(x) & n_1(x) \end{bmatrix} \tag{28a}$$

$$N_2(x) = \begin{Bmatrix} n_1(x) & n_2(x) \end{Bmatrix} \tag{28b}$$

$\mathbf{B}_1(x)$ and $\mathbf{B}_2(x)$ can be expressed as

$$\mathbf{B}_1(x) = \begin{bmatrix} \Phi_{,1}(x) & \mathbf{0} \\ \mathbf{0} & \Phi_{,2}(x) \\ \Phi_{,2}(x) & \Phi_{,1}(x) \end{bmatrix} \tag{29a}$$

$$\mathbf{B}_2(x) = \begin{bmatrix} \Phi_{,1}(x) \\ \Phi_{,2}(x) \end{bmatrix} \tag{29b}$$

$$\begin{Bmatrix} F^s_m(x,p) & F^s_e(x,p) & \begin{bmatrix} F^s_g(x,p) & F^s_\theta(x,p) \end{bmatrix} \end{Bmatrix}^T$$

is the load vector associated with the boundary conditions, the elements of which are

$$F^s_m(x,p) = -\int_{\Gamma_{st}} \tilde{\bar{t}}(x,p)\,d\Gamma \tag{30a}$$

$$F_e^s(x,p) = -\int_{\Gamma_{sD}} \tilde{\tilde{D}}(x,p)\, d\Gamma \tag{30b}$$

$$F_g^s(x,p) = -\int_{\Gamma_{sB}} \tilde{\tilde{B}}(x,p)\, d\Gamma \tag{30c}$$

$$F_\theta^s(x,p) = -\int_{\Gamma_{sq}} \tilde{\tilde{q}}(x,p)\, d\Gamma \tag{30d}$$

with Γ_{st}, Γ_{sD}, Γ_{sB} and Γ_{sq} being the parts of the local boundaries which coincide with the global stress, electric displacement, magnetic induction and heat flux boundaries, respectively.

The total system of equations can be obtained by superposing the corresponding ones of all the subdomains. And it can be expressed as

$$\mathbf{K}\hat{U} = F \tag{31}$$

where $\mathbf{K}$, $\hat{U}$, F, are the extended stiffness matrix, fictitious displacement vector and loading vector, respectively.

The displacements, electric potential, magnetic potential and temperature in the time domain can finally be obtained by applying the inverse Laplace transform technique. In the present work, the Stehfest's inversion algorithm [Stehfest (1970)] is used, i.e., if $\bar{f}(x,p)$ is known, the approximate value of $f(x,t)$ at a specific time t is given by

$$f(x,t) = \frac{\ln 2}{t} \sum_{i=1}^{M} v_i \bar{f}\left(x, \frac{\ln 2}{t} i\right) \tag{32}$$

where

$$v_i = (-1)^{M/2+i} \sum_{k=[i+1/2]}^{\min(i,M/2)} \frac{k^{M/2}(2k)!}{(M/2-k)!(k-1)!(i-k)!(2k-i)!} \tag{33}$$

5 The essential boundary conditions

Because the shape function of MLPG method lacks the delta function property, the essential boundary conditions can not be enforced directly. In this paper, a simple transformation technique presented in [Atluri et al. (1999)], which can transform the fictitious value $\hat{U}$ to actual value U in order to impose the essential boundary conditions directly, is adopted.

The MLS approximate values of all the nodes can be written as

$$U = \mathbf{\Phi}\hat{U} \tag{34}$$

where U is an extended displacement vector with $5N$ elements, and $\mathbf{\Phi}$ is the $5N \times 5N$ shape function matrix. From Eq. (34), we have

$$\hat{U} = \mathbf{\Phi}^{-1} U \tag{35}$$

Substituting Eq. (35) into Eq. (31), one obtains

$$\mathbf{K}\mathbf{\Phi}^{-1} U = F \tag{36}$$

Thus, the essential boundary conditions can be imposed through Eqs. (36). In fact, we do not need transform all the fictitious nodal values to the actual nodal ones. In order to alleviate the computational cost effectively, only the nodes with prescribed essential boundary conditions need to be considered, and the remainders of procedures are the same as the case of a full transformation given above.

6 Validation

To validate the proposed approach, numerical results are firstly compared with the possible analytical solutions. Consider a homogeneous magneto-electro-thermo-elastic square plate under a sudden heating on the top side. For the thermal field, the analytical solution can be obtained as

$$\theta(z,t) = 1 - \frac{4}{\pi} \sum_{n=0}^{\infty} \frac{(-1)^n}{2n+1} \exp\left[-\frac{(2n+1)^2 \pi^2 \kappa t}{4a^2} \right] \cos\left(\frac{(2n+1)\pi z}{2a} \right) \tag{37}$$

where a is the side-length of the plate and $\kappa = k_{33}/\rho c$ is the diffusivity coefficient. It should be remarked that the solution is the same as the one for homogeneous thermoelastic material [Carslaw and Jaeger (1959)]. In what follows, the magneto-electro-thermo-elastic solid is taken as $BaTiO_3$-$CoFe_2O_4$ composite with a volume fraction $V_f = 0.5$, and the material constants of which are taken as [Ootao and Tanigawa (2005)]

$$c_{11} = 226 \times 10^9 \mathrm{Nm}^{-2}, \quad c_{13} = 124 \times 10^9 \mathrm{Nm}^{-2}, \quad c_{33} = 216 \times 10^9 \mathrm{Nm}^{-2},$$

$$c_{44} = 44 \times 10^9 \mathrm{Nm}^{-2}, \quad e_{31} = -2.2 \mathrm{Cm}^{-2}, \quad e_{33} = 9.3 \mathrm{Cm}^{-2}, \quad e_{15} = 5.8 \mathrm{Cm}^{-2},$$

$$f_{31} = 290.2 \mathrm{N/Am}, \quad f_{33} = 350 \mathrm{N/Am}, \quad f_{15} = 275 \mathrm{N/Am},$$

$$\alpha_1 = 12.85 \times 10^{-6} 1/\mathrm{K}, \quad \alpha_2 = 12.85 \times 10^{-6} 1/\mathrm{K}, \quad \alpha_3 = 8.2 \times 10^{-6} 1/\mathrm{K},$$

$$\varepsilon_{11} = 5.64 \times 10^{-9} \mathrm{C}^2/\mathrm{Nm}^2, \quad \varepsilon_{33} = 6.35 \times 10^{-9} \mathrm{C}^2/\mathrm{Nm}^2,$$

$$g_{11} = 5.367 \times 10^{-12} \mathrm{Ns/VC}, \quad g_{33} = 2737.5 \times 10^{-12} \mathrm{Ns/VC},$$

$p_3 = 1.0 \times 10^{-4}\mathrm{C/m^2K}$,

$\mu_{11} = 297 \times 10^{-6}\mathrm{Ns^2C^{-2}}, \quad \mu_{33} = 83.5 \times 10^{-6}\mathrm{Ns^2C^{-2}}$,

$m_3 = 1.1 \times 10^{-4}\mathrm{N/AmK}$,

$k_{11} = 2.85\mathrm{W/Km}, \quad k_{33} = 2.85\mathrm{W/Km}$,

$\rho = 5.55 \times 10^{3}\mathrm{kg/m^3}, \quad c = 637\mathrm{Ws/kgK}$

It also should be pointed out that the pyromagnetic constant of the composite considered here is further assumed for the sake of calculation in this study.

The plate with a size of $a \times a = 1\mathrm{m} \times 1\mathrm{m}$ is discretized by 121 equidistantly distributed nodes for the MLS approximation. The nodal arrangement and boundary conditions are given in Fig. 1. The transient heat shock load on the top side of the plate is $T_0 H(t)$, where $H(t)$ is the Heaviside function. $T_0 = 1\mathrm{K}$ is assumed in all the numerical procedure including the next section.

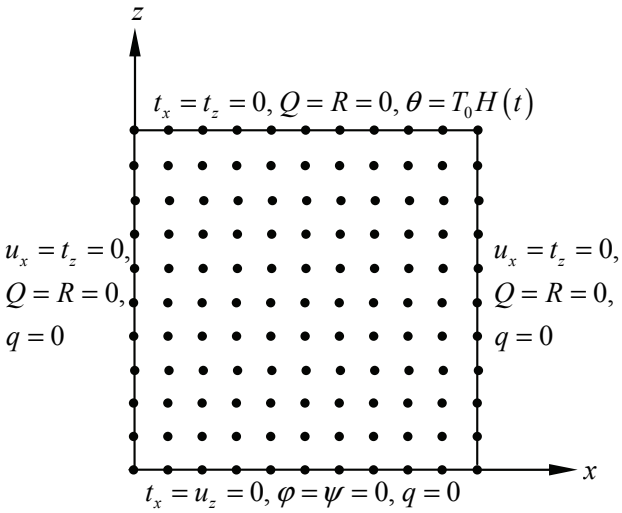

Figure 1: A magneto-electro-thermo-elastic square plate under thermal shock on the top side

As shown in Fig. 2, the calculated temperatures at the bottom and the mid-line of the plate are nearly the same as those obtained from the analytical solution given in Eq. (37) with a relative error 0.01%. Figs. 3 and 4, respectively, show the electric potential and magnetic potential calculated by the MLPG method and by FEM. For both the electric potential and magnetic potential, the agreements of the

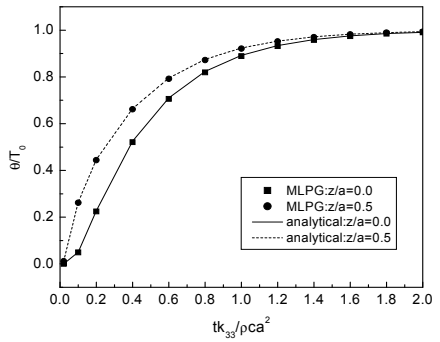

Figure 2: Normalized temperature increments at two different lines parallel to x-axis versus normalized time

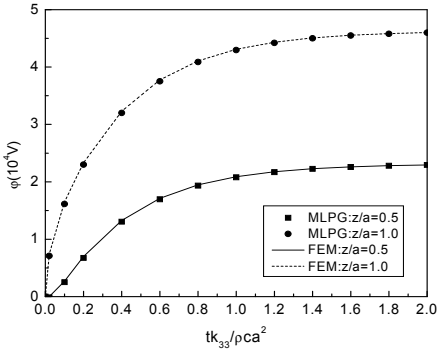

Figure 3: Electrical potentials at two different lines parallel to x-axis versus normalized time

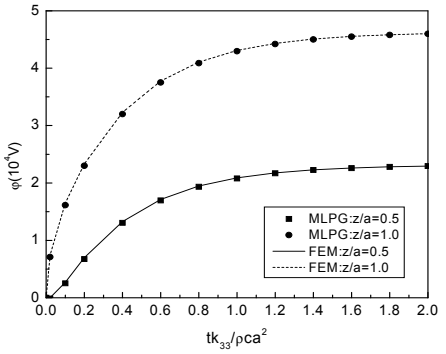

Figure 4: Magnetic potentials at two different lines parallel to x-axis versus normalized time

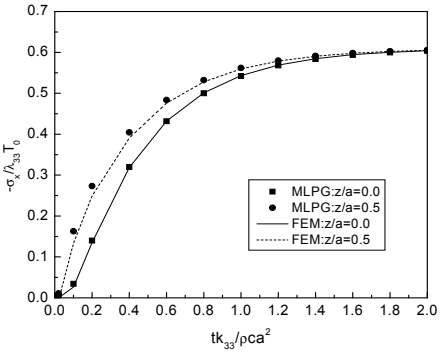

Figure 5: Normalized stresses at two different lines parallel to x-axis versus normalized time

numerical results by the two methods are excellent. A good agreement can also be observed for the calculated stress $-\sigma_x/\lambda_{33}T_0$ by the MLPG method and by FEM (Fig. 5). The comparisons between the results obtained by the present method and ones by the analytical solution or FEM confirm the accuracy and effectiveness of the present method.

The accuracy of the present method can also be verified by comparing the mode-I stress intensity factor of the reduced case of the present study with the one given by Sladek et al. (2007b) before. For example, for a central crack in a plate of thermo-piezoelectric PZT-5H with the same geometry as the one given by Sladek et al. (2007b), assume that the thermal load $T_0H(t)$ with $T_0 = 1$K is applied on the

outer boundary of the plate, and that vanishing value of temperature is kept on crack surfaces. As shown in Fig. 6, the results agree very well with the corresponding ones presented by Sladek et al. (2007b).

7 Dynamic fracture analysis of nonhomogeneous magneto-electro-thermo-elastic plates with cracks

7.1 An edge crack in a finite magneto-electro-thermo-elastic plate under thermal shock on the lateral side

For 2D plane crack problems of magnetoelectroelastic materials, the generalized field intensity factors (FIFs) including SIFs K_{II} and K_I, EDIF K_D and MIIF K_B are related to the displacements, electric potential and magnetic potential in the vicinity of crack tips, and they can be expressed as [Sladek et al. (2007b); García-Sánchez et al. (2007)]

$$\begin{Bmatrix} K_{II} \\ K_I \\ K_D \\ K_B \end{Bmatrix} = \sqrt{\frac{\pi}{2r}} \left[Re\left(\mathbf{\Xi}\right)^{-1} \right] \begin{Bmatrix} u_1 \\ u_3 \\ \phi \\ \psi \end{Bmatrix} \tag{38}$$

where the matrix $\mathbf{\Xi}$ is determined by the material properties. r is the radial polar coordinate with origin at the crack tip. The mechanical mode-I strain energy release rate (MSERR) can further be given as (Tian and Gabbert, 2004)

$$G_I^M = \frac{1}{4}\left(\Lambda_{21}K_IK_{II} + \Lambda_{22}K_IK_I + \Lambda_{23}K_IK_D + \Lambda_{24}K_IK_B\right) \tag{39}$$

where Λ_{ij} is the element of matrix $\mathbf{\Lambda}$ with $\mathbf{\Lambda} = \mathrm{Re}(\mathbf{\Xi})$.

In this section, an edge crack of length $a = 1.0$m in a nonhomogeneous magneto-electro-thermo-elastic plate with height $2h = 4.0$m and width $w = 2.0$m is considered. The plate is assumed to be subjected to a sudden temperature decrease T_0 on the left side (Fig. 7). Due to the symmetry, only half of the cracked plate is modeled for simplicity, and 441 equidistantly distributed nodes are employed for the MLPG method. For the nonhomogeneous material considered here, the material constants at $z = 0$ are taken as the corresponding ones of $BaTiO_3$-$CoFe_2O_4$ composite with a volume fraction $V_f = 0.5$ (listed before). And all the material parameters are firstly assumed to vary continuously along the z-direction in the following form:

$$\Pi(z) = \Pi_0 \exp(\beta\,|z|) \tag{40}$$

where Π_0 denotes the corresponding material parameters at $z = 0$, andβ is the introduced nonhomogeneous parameter.

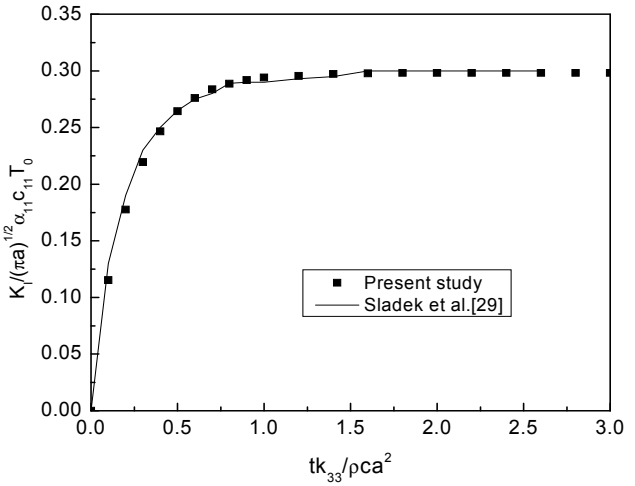

Figure 6: Normalized SIF of a central crack in a thermo-piezoelectric plate

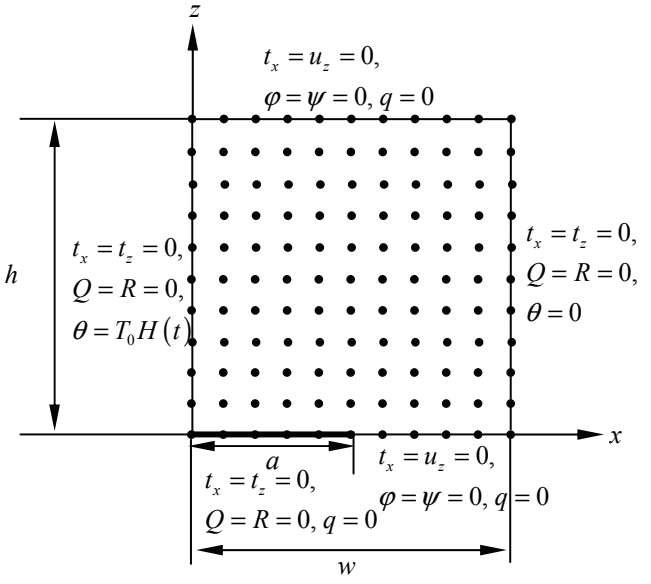

Figure 7: An edge crack in a finite nonhomogeneous magneto-electro-thermo-elastic plate under a thermal shock on the lateral side

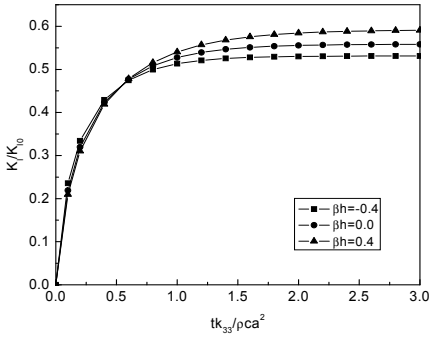

Figure 8: Normalized SIF of an edge crack versus normalized time for different nonhomogeneous parameter βh

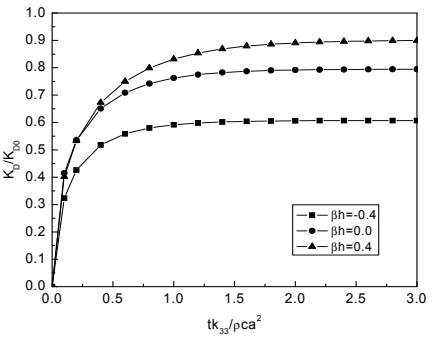

Figure 9: Normalized EDIF of an edge crack versus normalized time for different nonhomogeneous parameter βh

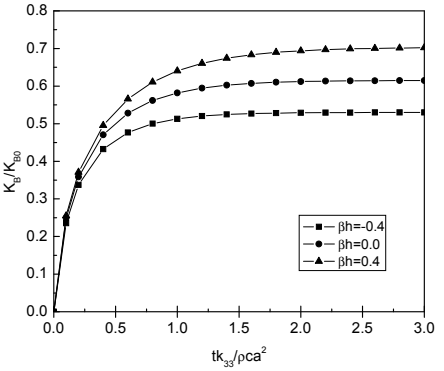

Figure 10: Normalized MIIF of an edge crack versus normalized time for different nonhomogeneous parameter βh

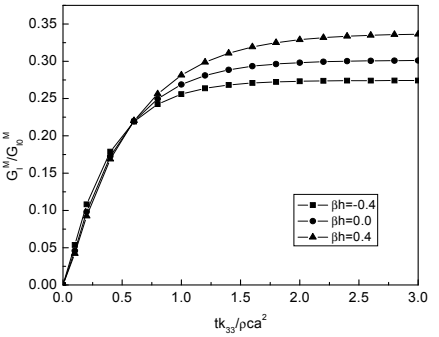

Figure 11: Normalized MSERR of an edge crack versus normalized time for different nonhomogeneous parameter βh

Figs. 8 to 11 show the effects of normalized nonhomogeneous parameter βh on the normalized FIFs and MSERR, where

$$K_{I0} = \left(\lambda_{11} c_{13}/c_{11} - \lambda_{33}\right) T_0 \sqrt{\pi a} \tag{41a}$$

$$K_{D0} = \left(\lambda_{11} e_{31}/c_{11} + p_3\right) T_0 \sqrt{\pi a} \tag{41b}$$

$$K_{B0} = \left(\lambda_{11} f_{31}/c_{11} + m_3\right) T_0 \sqrt{\pi a} \tag{41c}$$

and

$$G_{I0}^M = \frac{\pi a}{4} \Lambda_{22} \left(\lambda_{11} c_{13}/c_{11} - \lambda_{33}\right)^2 T_0^2 \tag{42}$$

As shown in these figures, the steady values of both the FIFs and MSERR increase with the increasing of βh. Furthermore, the times for them to reach their corresponding steady values slightly increase as well with the increasing of βh. Fig. 11 implies that according to energy release rate criterion, decreasing the nonhomogeneous parameter can impede the crack propagation and growth. Similar phenomenon is, in fact, observed by Ueda (2004) before for an edge crack problem in a nonhomogeneous piezoelectric strip.

Different material parameters perhaps have different effects on the fracture behaviors of the cracks. As well known, the MSERR is an important fracture parameter of magnetoelectroelastic materials. Thus, in what follows, the effects of a single thermal material parameter on the MSERR are respectively evaluated emphatically. For the sake of convenience, the following expressions are introduced:

$$\lambda_{11} = \lambda_{110} \exp(\beta_1 |z|) \tag{43a}$$

$$\lambda_{33} = \lambda_{330} \exp(\beta_2 |z|) \tag{43b}$$

$$p_3 = p_{30} \exp(\beta_3 |z|) \tag{43c}$$

$$m_3 = m_{30} \exp(\beta_4 |z|) \tag{43d}$$

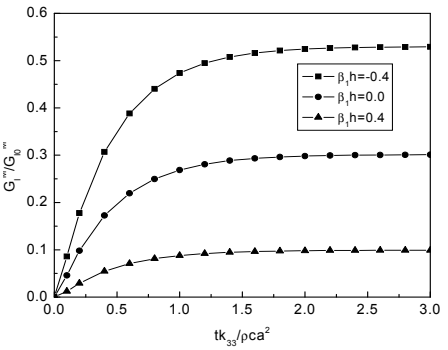

Figure 12: Normalized MSERR of an edge crack versus normalized time for different nonhomogeneous parameter $\beta_1 h$

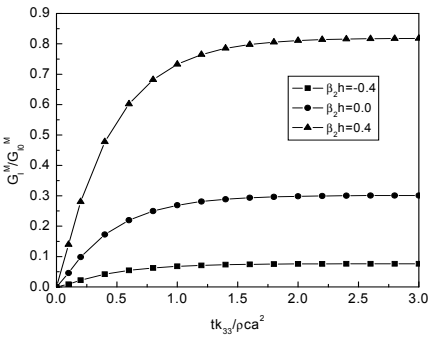

Figure 13: Normalized MSERR of an edge crack versus normalized time for different nonhomogeneous parameter $\beta_2 h$

It should be pointed out that except for $\beta_1 h$ in Fig. 12, $\beta_2 h$ in Fig. 13, $\beta_3 h$ in Fig. 14 and $\beta_4 h$ in Fig. 15; the other material parameters are kept to be the corresponding ones of $BaTiO_3$-$CoFe_2O_4$. It is easily seen from Fig. 12 to 15 that the MSERR

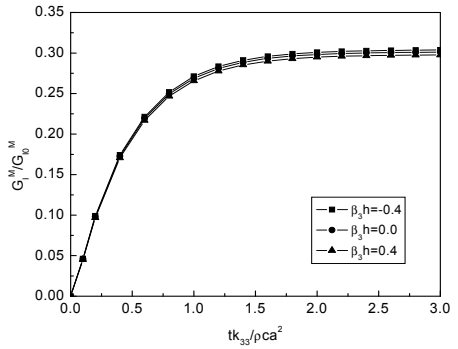

Figure 14: Normalized MSERR of an edge crack versus normalized time for different nonhomogeneous parameter $\beta_3 h$

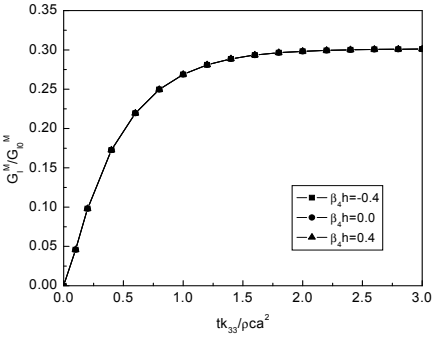

Figure 15: Normalized MSERR of an edge crack versus normalized time for different nonhomogeneous parameter $\beta_4 h$

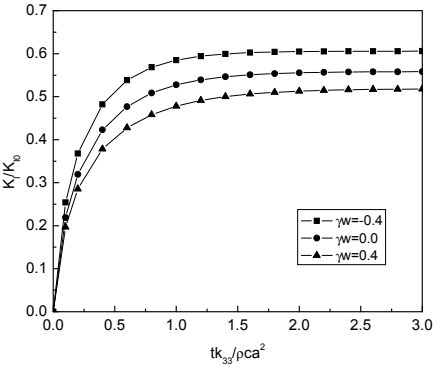

Figure 16: Normalized SIF of an edge crack versus normalized time for different nonhomogeneous parameter γw

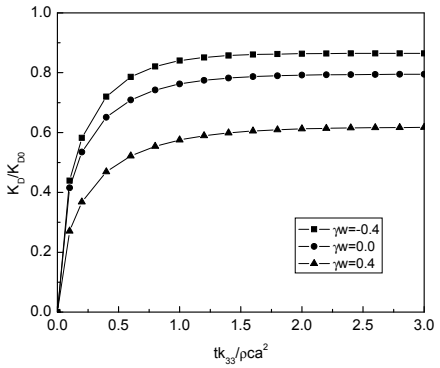

Figure 17: Normalized EDIF of an edge crack versus normalized time for different nonhomogeneous parameter γw

decreases with the increasing of either $\beta_1 h$ or $\beta_3 h$, the MSERR increases with the increasing of $\beta_2 h$, and that the MSERR has no obvious variance for different $\beta_4 h$. Thus, according to energy release rate criterion, the larger λ_{11} is, the more stable the crack is. Increasing p_3 will slightly retard the crack extension as well. On the contrary, decreasing λ_{33} will impede the crack propagation and growth. However, it is not easy to impede the crack initiation by adjusting the material parameter m_3.

In order to examine the effect of the vary direction of material properties on the thermal shock, the case of varying material properties in the x direction is also

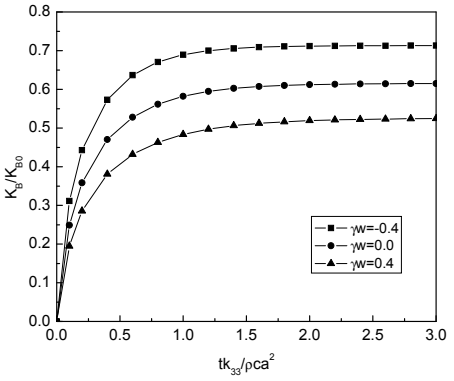

Figure 18: Normalized MIIF of an edge crack versus normalized time for different nonhomogeneous parameter γw

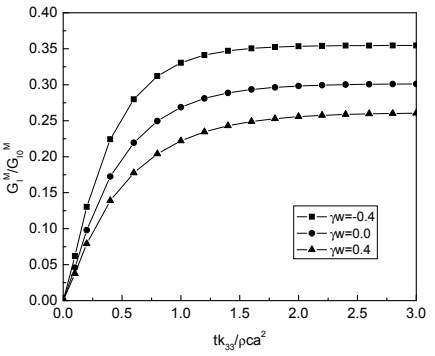

Figure 19: Normalized MSERR of an edge crack versus normalized time for different nonhomogeneous parameter γw

considered. The material parameters are assumed as

$$\Sigma(x) = \Sigma_0 \exp(\gamma x) \tag{44}$$

where Σ_0 denotes the corresponding material properties at $x = 0$, and γ is the nonhomogeneous parameter in the x direction.

The effects of normalized nonhomogeneous parameter γw on the normalized FIFs and MSERR are shown in Figs. 16-19. Contrary to the case of the material parameters changing along the z direction, FIFs and MSERR decreasing with the increasing of γw. It means that increasing the nonhomogeneous parameters along x direction can inhibit the crack growth and weaken the effect of the thermal shock.

7.2 A central crack in a finite magneto-electro-thermo-elastic plate under thermal shock on the top side

In this section, a central crack of length $2a$ in a finite magneto-electro-thermo-elastic plate is analyzed. The plate's width, height and the crack's length are respectively $2w = 4.0\,\mathrm{m}$, $2h = 4.0\,\mathrm{m}$ and $2a = 2.0\,\mathrm{m}$. Taking advantage of symmetry, only a quarter of the plate is modeled. The geometry of the considered model is given in Fig. 20. For the MLS approximation, 441 equidistantly distributed nodes are used. The nodal arrangement and boundary conditions are also displayed in Fig. 20. Limited by the length of this paper, only some typical numerical results are given in this section.

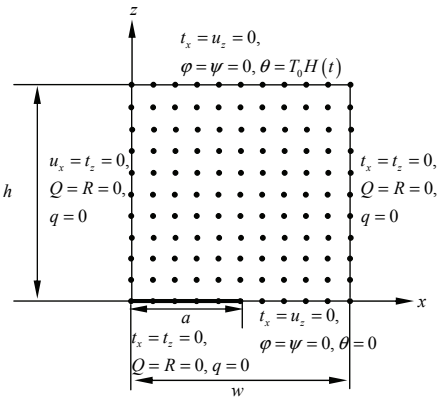

Figure 20: A central crack in a finite nonhomogeneous magneto-electro-thermo-elastic plate under a thermal shock on the top side

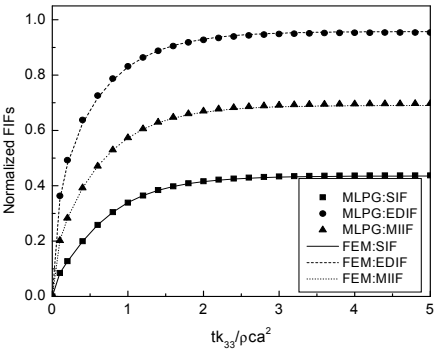

Figure 21: Comparison between the normalized FIFs of a central crack in a homogeneous magneto-electro-thermo-elastic plate obtained by MLPG method and the corresponding ones by FEM

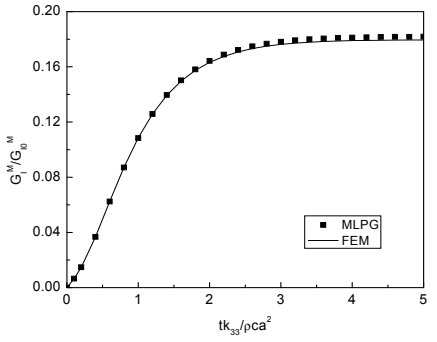

Figure 22: Comparison between the normalized MSERR of a central crack in a homogeneous magneto-electro-thermo-elastic plate obtained by MLPG method and the corresponding ones by FEM

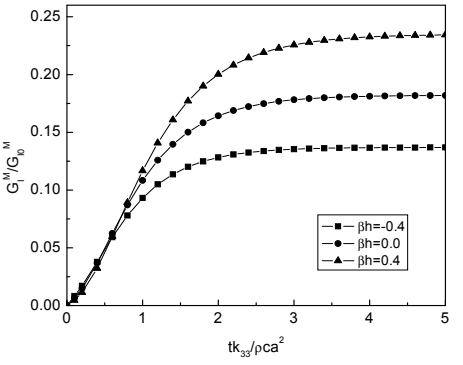

Figure 23: Normalized MSERR of a central crack versus normalized time for different nonhomogeneous parameter βh

Figs. 21 and 22, respectively, show the normalized FIFs and MSERR of the central crack situated in a homogeneous magneto-electro-thermal-elastic plate subjected to thermal shock on the top side. And for comparison, the corresponding results obtained by FEM are plotted in these figures simultaneously. It is easily seen from

these figures that similar to an edge crack, there is a good coincidence between the results given by MLPG method and the ones by FEM.

Fig. 23 presents the effects of the nonhomogeous parameterβ(defined in Eq. (40)) on the normalized MSERR. It is found that similar to the case of an edge crack, the MSERR increase with increasing of βh. However, comparing Fig. 23 with Fig. 11, it is noted that the times that the normalized MSERR of a central crack reaching the corresponding steady values are much longer than the corresponding ones of an edge crack.

8 Conclusions

The fracture problems of nonhomogeneous magneto-electro-thermo-elastic plate under thermal shock are investigated by the meshless local Petrov-Galerkin method. The material parameters are assumed to vary in either the height or width direction. Both the FIFs and mechanical mode-I MSERR of cracks in the magneto-electro-thermo-elastic plates are calculated. The following conclusions can be drawn.

(1). MLPG method is an effective numerical method to treat the coupling problem of nonhomogeneous magneto-electro-thermo-elasticity under thermal shock.

(2). For either edge crack or central crack problems of nonhomogeneous magneto-electro-thermo-elastic plate under a definite thermal shock, according to the maximum energy release rate criterion, both decreasing the nonhomogeneous parameter defined by βh and increasing the nonhomogeneous parameter defined by γw will impede crack initiation and growth.

(3). According to energy release rate criterion, both increasing λ_{11} and p_3 will retard the crack propagation and growth. On the other hand, decreasing λ_{33} can also impede crack to initiate and grow. However, adjusting m_3 has insignificant effects on the fracture behaviors.

(4). For a central crack in a finite magneto-electro-thermo-elastic plate, the times that the normalized MSERRs reach their steady values are much longer than the corresponding ones for the case of an edge crack.

Acknowledgement: Dr. W.J. Feng would like to give his sincere thanks to the editor and the reviewers for their suggestions to improve the presentation of the wok. The work was supported by Natural Science Fund of China (10772123) and Natural Science Fund for Outstanding Youngers of Hebei Province (2009001624), China.

References

Atluri, S.N. (2004): *The meshless method (MLPG) for domain & BIE discretizations*. Tech Science Press.

Atluri, S.N.; Kim, H.G.; Cho, J.Y. (1999): A critical assessment of the truly meshless local Petrov-Galerkin (MLPG) and local boundary integral equation (LBIE) methods. *Comput. Mech.,* 24: 348-372.

Atluri, S.N.; Shen, S.P. (2002a): *The Meshless Local Petrov-Galerkin (MLPG) Method*. Tech Science Press.

Atluri S.N.; Shen S.P. (2002b): The meshless local Petrov-Galerkin (MLPG) method: A simple & less costly alternative to the finite element and boundary element methods. *CMES: Computer Modeling in Engineering & Sciences*, 3: 11-51.

Atluri, S.N.; Zhu, T. (1998): A New Meshless Local Petrov-Galerkin (MLPG) Approach in Computational Mechanics. *Comput. Mech.,* 22: 117-127.

A**vellaneda, M.; Harshe, G.** (1994): Magnetoelectric effect in piezoelectric/magnetostrictive multilayer (2-2) composites. *J. Intell. Mater. Syst. Struct.*, 5: 501–513.

Batra, R.C.; Ching, H.K. (2002): Analysis of Elastodynamic Deformations near a Crack/Notch Tip by the Meshless Local Petrov-Galerkin (MLPG) Method. *CMES: Computer Modeling in Engineering & Sciences*, 3: 717-730.

Benveniste, Y. (1995): Magnetoelectric effect in fibrous composites with piezoelectric and piezomagnetic phases. *Phys. Rev. B*, 51: 16424–16427.

Carslaw, H.S.; Jaeger, J.C. (1959): *Conduction of Heat in Solids.* Oxford University Press, Oxford.

Ching, H.K.; Chen, J.K. (2006): Thermomechanical Analysis of Functionally Graded Composites under Laser Heating by the MLPG Method. *CMES: Computer Modeling in Engineering & Sciences*, 13: 199-218.

Ching, H.K.; Yen, S.C. (2005): Meshless local Petrov-Galerkin analysis for 2D functionally graded elastic solids under mechanical and thermal loads. *Compos. Part B: Eng.*, 36: 223-240.

Feng, W.J.; Pan, E. (2008): Dynamic fracture behavior of an internal interfacial crack between two dissimilar magneto-electro-elastic plates. *Eng. Fract. Mech.*, 75: 1468–1487.

Feng, W.J.; Pan, E.; Wang, X. (2007): Dynamic fracture analysis of a penny-shaped crack in a magnetoelectroelastic layer. *Int. J. Solids Struc*t., 44, 7955–7974.

Feng, W.J.; Pan, E.; Wang, X. (2008): Stress analysis of a penny-shaped crack in a magneto-electro-thermo-elastic layer under uniform heat flow and shear loads. *J. Therm. Stress.,* 31: 497-514.

Gao, C.F.; Kessler, H.; Balke, H. (2003a): Crack problems in magnetoelectroelastic solids. Part I: exact solution of a crack. *Int. J. Eng. Sci.,* 41: 969–981.

Gao, C.F.; Kessler, H.; Balke, H. (2003b). Crack problems in magnetoelectroelastic solids. Part II: general solution of collinear cracks. *Int. J. Eng. Sci.,* 41: 983–994.

Gao, C.F.; Kessler, H.; Balke, H. (2003c). Fracture analysis of electromagnetic thermoelastic solids. *Eur. J. Mech. A/Solids,* 22: 433–442.

Gao, L.; Liu, K.; Liu, Y. (2006): Applications of MLPG Method in Dynamic Fracture Problems. *CMES: Computer Modeling in Engineering & Sciences*, 12: 181-196.

García-Sánchez, F.; Rojas-Díaz, R.; Sáez, A. Zhang, Ch. (2007): Fracture of magnetoelectroelastic composite materials using boundary element method (BEM). *Theor. Appl. Fract. Mech.,* 47: 192-204.

Han, Z. D.; Atluri, S. N. (2003): Truly meshless local Petrov-Galerkin (MLPG) solutions of traction & displacement BIEs. *CMES: Computer Modeling in Engineering & Sciences*, 4: 665-678.

Han, Z. D.; Atluri, S. N. (2004a): Meshless local Petrov-Galerkin (MLPG) approaches for solving 3D Problems in elasto-statics. *CMES: Computer Modeling in Engineering & Sciences*, 6: 169-188.

Han, Z. D.; Atluri, S. N. (2004b): A meshless local Petrov-Galerkin (MLPG) approach for 3-Dimensional elasto-dynamics. *CMC: Computers, Materials & Continua*, 1: 129-140.

Han, Z.D.; Liu, H.T.; Rajendran, A.M.; Atluri, S.N. (2006): The applications of Meshless Local Petrov-Galerkin (MLPG) approaches in high-speed impact, penetration and perforation problems. *CMES: Computer Modeling in Engineering & Sciences*, 14: 119-128.

Huang, J.H.; Kuo, W.S. (1997): The analysis of piezoelectric/piezomagnetic composite materials containing ellipsoidal inclusions. *J. Appl. Phys*., 81: 1378–1386.

Jarak, T.; Soric, J.; Hoster, J. (2007): Analysis of Shell Deformation Responses by the Meshless Local Petrov-Galerkin (MLPG) Approach. *CMES: Computer Modeling in Engineering & Sciences*. 18: 235-246.

Krysl, P.; Belytschko, T. (1995): Analysis of thin plates by the element-free Galerkin method. *Comput. Mech*., 17: 26-35.

Lancaster, P.; Salkauskas, K. (1981): Surfaces generated by moving least squares methods. *Math. Comput*., 37: 141-158.

Li, J.Y. (2000): Magnetoelectroelastic multi-inclusion and inhomogeneity problems and their applications in composite materials. *Int. J. Eng. Sci.,* 38: 1993–

2011.

Li, Q.; Shen, S.; Han, Z. D.; Atluri, S. N. (2003): Application of meshless local Petrov-Galerkin (MLPG) to problems with singularities, and material discontinuities, in 3-D elasticity, *CMES: Computer Modeling in Engineering& Sciences*, 4: 567-581.

Li, X.F. (2005): Dynamic analysis of a cracked magnetoelectroelastic medium under antiplane mechanical and inplane electric and magnetic impacts. *Int. J. Solids Struct.,* 42: 3185–3205.

Long, S.Y.; Liu, K.Y.; Li, G.Y. (2008): An analysis for the elasto-plastic fracture problem by the meshless local Petrov-Galerkin method. *CMES: Computer Modeling in Engineering& Sciences*, 28: 203-216.

Nan, C.W. (1994): Magnetoelectric effect in composites of piezoelectric and piezomagnetic phases. *Phys. Rev. B*, 50: 6082–6088.

Niraula, O.P.; Wang, B.L. (2006): Thermal stress analysis in magneto-electro-thermo-elasticity with a penny-shaped crack under uniform heat flow. *J. Therm. Stress.,* 29: 423-437.

Ootao, Y.; Tanigawa, Y. (2005): Transient analysis of multilayered magneto-electro-thermoelastic strip due to nonuniform heat supply. *Compos. Struct.*, 68: 471-480.

Qian, L.F.; Batra, R.C. (2005): Three-dimensional transient heat conduction in a functionally graded thick plate with a higher-order plate theory and a meshless local Petrov-Galerkin method. *Comput. Mech.*, 35: 214-226.

Sellountos, E.J.; Vavourakis, V.; Polyzos, D. (2005): A new singular/hypersingular MLPG (LBIE) method for 2D elastostatics. *CMES: Computer Modeling in Engineering & Sciences*, 7: 35-48.

Sladek, J.; Sladek, V.;Wen, P.H.; Aliabadi, M.H. (2006a): Meshless Local Petrov-Galerkin (MLPG) Method for Shear Deformable Shells Analysis. *CMES: Computer Modeling in Engineering & Sciences*, 13: 103-118.

Sladek, J.; Sladek, V.; Zhang, Ch.; Tan, C.L. (2006b): Meshless Local Petrov-Galerkin Method for Linear Coupled Thermoelastic Analysis. *CMES: Computer Modeling in Engineering & Sciences*, 16: 57-68.

Sladek, J.; Sladek, V.; Zhang, Ch.; Solek, P.; Starek, L. (2007a): Fracture analyses in continuously nonhomogeneous piezoelectric solids by the MLPG. *CMES: Computer Modeling in Engineering & Sciences*, 19: 247-262.

Sladek, J.; Sladek, V.; Zhang, Ch.; Solek, P. (2007b): Application of the MLPG to thermo-piezoelectricity. *CMES: Computer Modeling in Engineering & Sciences*, 22: 217-233.

Sladek, J.; Sladek, V.; Tan, C.L.; Atluri, S.N. (2008a): Analysis of Transient Heat Conduction in 3D Anisotropic Functionally Graded Solids, by the MLPG Method. *CMES: Computer Modeling in Engineering & Sciences*, 32: 161-174.

Sladek, J.; Sladek, V.; Solek, P.; Saez, A. (2008b): Dynamic 3D axisymmetric problems in continuously non-homogeneous piezoelectric solids. *Int. J. Solids Struct.*, 45: 4523-4542.

Sladek, J.; Sladek, V.; Solek, P.; Atluri, S.N. (2008c): Modeling of Intelligent Material Systems by the MLPG. *CMES: Computer Modeling in Engineering & Sciences*, 34: 273-300.

Song, Z.F.; Sih, G.C. (2003): Crack initiation behavior in magnetoelectroelastic composite under in-plane deformation. *Theor. Appl. Fract. Mech.,* 39: 189–207.

Stehfest, H. (1970): Algorithm 368: numerical inversion of Laplace transform. *Commun. Assoc. Comput. Mach.,* 13: 47-49.

Tian, W.Y.; Gabbert, U. (2004): Multiple crack interaction problems in magneto-electroelastic solids. *Eur. J. Mech. A/Solids,* 23: 599–614.

Ueda, S. (2004): Thermally induced fracture of a functionally graded piezoelectric layer. *J. Therm. Stress.,* 27: 291-309.

Van Suchtelen, J. (1972): Product properties: a new application of composite materials. *Phillips Research Reports,* 27: 28–37.

Wang, B.L.; Mai, Y.W. (2007): Applicability of the crack-face electromagnetic boundary conditions for fracture of magnetoelectroelastic materials. *Int. J. Solids Struct.,* 44: 387-398.

Zhao, M.H.; Yang, F.; Liu, T. (2006): Analysis of a penny-shaped crack in a magneto-electro-elastic medium. *Phil. Mag.,* 86: 4397-4416.

Zhou, Z.G.; Wu, L.Z.; Wang, B. (2005): The behavior of a crack in functionally graded piezoelectric/piezomagnetic materials under anti-plane shear loading. *Arch. Appl. Mech.*, 74: 526-535.